PREPARED FOR THE U.S. DEPARTMENT OF ENERGY,
UNDER CONTRACT DE-AC02-76-CHO-3073

PPPL-2851
UC-427

PPPL-2851

A FULLY NONLINEAR CHARACTERISTIC METHOD FOR GYROKINETIC SIMULATION

BY

S.E. PARKER AND W.W. LEE

July, 1992

PPPL PRINCETON PLASMA PHYSICS LABORATORY

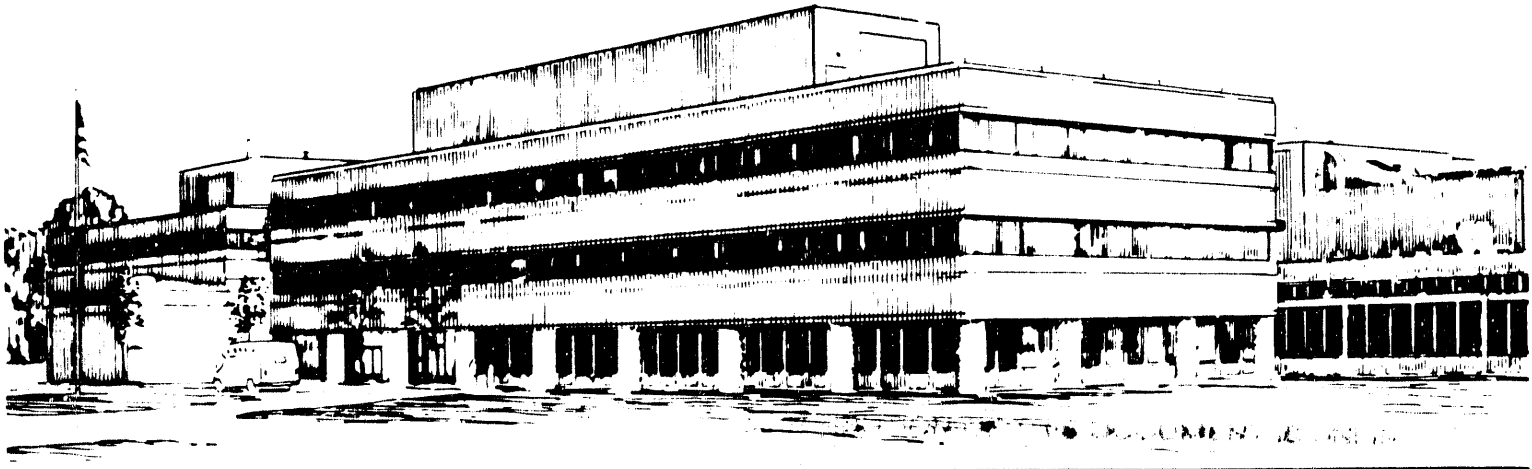

PRINCETON UNIVERSITY, PRINCETON, NEW JERSEY

NOTICE

NOTICE

PPPL--2851

DE92 016803

A Fully Nonlinear Characteristic Method for Gyrokinetic Simulation

S. E. Parker and W. W. Lee

Princeton Plasma Physics Laboratory, Princeton University

Princeton, NJ 08543

Abstract

We present a new scheme which evolves the perturbed part of the distribution function along a set of characteristics that solves the fully nonlinear gyrokinetic equations. This nonlinear characteristic method for particle simulation is an extension of the partially linear weighting scheme,[1] and may be considered an improvement of existing δf methods.[2,3] Some of the features of this new method are: the ability to keep all the nonlinearities, particularly those associated with parallel acceleration; the loading of the physical equilibrium distribution function f_0 (e.g., a Maxwellian), with or without the multiple spatial scale approximation;[4] the use of a single set of trajectories for the particles; and also, the retention of the conservation properties of the original gyrokinetic system in the numerically converged limit (i.e., small Δt, small Δx and a large number of particles). Therefore, one can take advantage of the low noise property of the weighting scheme together with the quiet start techniques to simulate weak instabilities, with a substantially reduced number of particles than required for a conventional simulation. The new method is used to study a one dimensional drift wave model which isolates the parallel velocity nonlinearity. A mode coupling calculation of the saturation mechanism is given, which is in good agreement with the simulation results and predicts a considerably lower saturation level then the estimate of Sagdeev and Galeev.[5] Finally, we extend the nonlinear characteristic method to the electromagnetic gyrokinetic equations in general geometry.

I. Introduction

An outstanding issue in gyrokinetic simulation (and in particle-in-cell simulation in general) is that often times it is necessary to use a rather large number of particles to resolve the physics of interest. The concern being that thermal fluctuations (or noise) and lack of sampling (or resolution) of the two to six dimensional phase space caused by a finite number of particles may obscure the physical process being modeled. For example, the broad-band density fluctuations existing in tokamak plasmas usually have an average level of a fraction of one percent or less. Thus, modeling such plasmas requires a very large number of particles for proper resolution, such that $N_{tot} \gg 1/(\delta n/n)^2 \approx 10^6$.[4] Early on it was recognized by Beyers and others that improvements in noise properties could be made by loading more uniform distributions or "quiet starts,"[6-8] and also by linearization techniques which track the perturbed quantities in terms of the equilibrium trajectories.[9,10] More recently, Dimits and Lee[1] developed a linear and a "partially linear" scheme by allowing the particle weights to evolve in time. In the linear scheme the particle weights follow the equilibrium trajectories. In the partially linearized scheme, the $E \times B$ nonlinearity is retained by adding this drift to the equilibrium (zeroth-order) orbit. There have been other investigations[2,3] into similar techniques often called δf methods, but no schemes up to this point have reported actual simulation results where the parallel velocity nonlinearity is retained.

The nonlinear characteristic method presented here is similar to previous weighting schemes;[1] however, the fully nonlinear trajectories are evolved and a consistent evolution equation is used for the particle weights. We begin by presenting the new method for the electrostatic slab case and the associated conservation properties of particle number, momentum, and total energy. We then present gyrokinetic simulations of a simple one dimensional drift wave instability in a shearless slab. This model isolates $E_{\|}\partial_{v_{\|}}\delta f$ nonlinearity and allows us to study the associated nonlinear physics. A three wave mode coupling theory is presented which gives a saturation level of $e|\phi|/T_e \approx 5.5\gamma^2/(k_{\|}v_{te})^2$ which is much lower than the calculation of Sagdeev and Galeev,[5] $e|\phi|/T_e \approx \frac{1}{4}(k_{\perp}\rho_s)^2$. There is good agreement between theory and simulation in terms of linear frequency, growth rate, and

nonlinear saturation. The conservation properties of the simulation plasma have also been investigated. It is found that the conservation of number density, momentum and energy in the nonlinear stages of the simulation can be achieved only if we use a sufficiently large number of particles, small timesteps, and a small grid cell size. Finally, we discuss the application of the nonlinear characteristic method to the general electromagnetic (nonuniform equilibrium magnetic field) gyrokinetic equations.

II. Nonlinear Characteristic Method

As mentioned earlier, devising a scheme where only the perturbed part of the distribution function is evolved has been previously investigated.[1-3] It was recognized that, by evolving only the perturbed part of the distribution δf, one could remove the initial noise associated with the equilibrium f_0 due to the use of a finite number of particles.[6] The scheme we present here is similar to the previously proposed δf methods,[2,3] but we take into account the discrete representation of the characteristics in a similar fashion as was done for the linear and partially linearized schemes.[1]

Let us begin by writing the distribution function $f(\mathbf{R}, v_{||}, \mu)$ in the familiar way as $f = f_0 + \delta f$, where f_0 is the equilibrium background distribution and is independent of time, and δf is the perturbed time dependent part of the distribution. For $(k_\perp \rho_i)^2 \ll 1$, the gyrokinetic equation for δf in the electrostatic slab limit is

$$\partial_t \delta f + \mathbf{v}_E \cdot \nabla \delta f + v_{||} \nabla_{||} \delta f + \frac{q}{m} E_{||} \partial_{v_{||}} \delta f = -\mathbf{v}_E \cdot \nabla f_0 - \frac{q}{m} E_{||} \partial_{v_{||}} f_0. \tag{1}$$

where $\rho_i \equiv v_{ti}/\Omega_i$ is the ion gyroradius, $\mathbf{v}_E \equiv c\mathbf{E}/B \times \hat{\mathbf{b}}$ is the $\mathbf{E} \times \mathbf{B}$ drift. The corresponding gyrokinetic Poisson equation in the small $(k_\perp \rho_i)^2$ limit is

$$(\rho_s/\lambda_D)^2 \nabla_\perp^2 \phi = -4\pi e(n_i - n_e), \tag{2}$$

where $\rho_s \equiv \sqrt{\tau}\rho_i$, $\tau \equiv T_e/T_i$, $\lambda_D \equiv \sqrt{T_e/(4\pi n_0 e^2)}$ is the Debye length, and

$$n = \int \delta f dv_{||} d\mu. \tag{3}$$

The characteristics (or trajectories) of Eq. (1) are

$$\dot{v}_{\|} = \frac{q}{m} E_{\|}, \tag{4}$$

$$\dot{\mathbf{R}} = v_{\|}\hat{\mathbf{b}} + \mathbf{v}_E, \tag{5}$$

and along these characteristics δf is changing because the right hand side of Eq. (1) is nonzero (note that $\dot{\mu} = 0$ here). The evolution equation for δf along the trajectories is

$$\dot{\delta f} = -\mathbf{v}_E \cdot \nabla f_0 - \frac{q}{m} E_{\|} \partial_{v_{\|}} f_0. \tag{6}$$

Now, we simply need to solve Eqs. (4)-(6). At first glance, one might consider loading a large number of characteristics (or particles), each having it's own δf, evolve the system in time and then weight the δf's to the grid to obtain field quantities. However, one needs to examine carefully how δf is being numerically represented and whether Eq. (1) or (6) is indeed being solved correctly.

In a similar fashion as the partially linear weighting scheme,[4] except now the fully nonlinear trajectories are evolved, δf in the simulation is represented as

$$\delta f(\mathbf{R}, v_{\|}, \mu, t) = \sum_{i=1}^{N} w_i S(\mathbf{R} - \mathbf{R}_i)\delta(v_{\|} - v_{\|i})\delta(\mu - \mu_i). \tag{7}$$

where N is the total number of particles and S is the particle shape function. w_i is the particle weight and can be interpreted as the $\delta f/f$ associated with the particle i, as will be shown below. $S(u) = \delta(u)$ is used for present discussion (i.e., we assume the particle shape function has the same properties as the delta function). This is equivalent to assuming that all quantities have a small spatial (or long wavelength) variation compared to the particle size. One can then use relations such as the following

$$\sum_i f(\mathbf{R}_i) S(\mathbf{R} - \mathbf{R}_i) = \sum_i [f(\mathbf{R}) - (\mathbf{R} - \mathbf{R}_i) \cdot \nabla f(\mathbf{R}) + \cdots] S(\mathbf{R} - \mathbf{R}_i) \tag{8}$$

$$\approx f(\mathbf{R}) \sum_i S(\mathbf{R} - \mathbf{R}_i). \tag{9}$$

Substituting Eq. (7) into Eq. (1) we obtain the following relation,

$$\sum_i \dot{w}_i \delta(\mathbf{R} - \mathbf{R}_i)\delta(v_{\|} - v_{\|i})\delta(\mu - \mu_i) = -\mathbf{v}_E \cdot \nabla f_0 - \frac{q}{m} E_{\|} \partial_{v_{\|}} f_0. \tag{10}$$

It should be noted here that Eq. (10) and Eq. (6) are quite different. Namely, the evolution of $\dot{w}$ from Eq. (10) is not the same as assuming $\dot{w} = \delta\dot{f}$ and using Eq. (6) to evolve w along it's trajectory. We will elaborate this point later. Next, we assume that the particle distribution can be represented as a smooth analytical function

$$g(\mathbf{R}, v_{\|}, \mu, t) \approx \sum_i \delta(\mathbf{R} - \mathbf{R}_i)\delta(v_{\|} - v_{\|i})\delta(\mu - \mu_i). \tag{11}$$

(g could be equal to the physical distribution f, but this is not necessary up to this point.) From Eqs. (10) and (11), we obtain

$$\dot{w}_i = -\left[\mathbf{v}_E \cdot \frac{\nabla f_0}{g} + \frac{q}{m} E_{\|} \frac{\partial_{v_{\|}} f_0}{g}\right]_{\mathbf{R}=\mathbf{R}_i, v_{\|}=v_{\|i}, \mu=\mu_i, t}. \tag{12}$$

One way to solve Eq. (12) is to note that the function g satisfies the full nonlinear gyrokinetic equation so that g is constant along a trajectory. One then can use the relation $g(\mathbf{R}_i, v_{\|i}, \mu_i, t) = g\left[\mathbf{R}_i(t=0), v_{\|i}(t=0), \mu_i, t=0\right]$. Since the initial loading is arbitrary, one can, for example, load a uniform distribution $g(t=0) = const.$ independent of the phase space variables, which seems to be the approach proposed by Kotschenruether.[3]

However, the equilibrium f_0 with a nonuniform loading in the velocity space (with or without spatial inhomogeneity) is preferred, because one wants more phase space resolution (i.e., particles) where the wave is in resonance with the distribution function ($\omega/k_{\|} = v_{\|}$). Typically, for low frequency microinstabilities, the resonant velocities are smaller than the thermal velocity of the species. Thus, a nonuniform loading (e.g., the Maxwellian distribution) in velocity space is much more desirable than a uniform one. One problem associated with the nonuniform loading for the existing δf schemes is that additional particle arrays (or calculations) are needed to keep track of $g_i(t=0)$. Moreover, numerical difficulties may arise from the denominators of Eq. (12) for particles with small values of $g_i(t=0)$, i.e., those initially located in the tail of the distribution. These are the potential drawbacks for using Eq. (12) to evaluate w_i, along with $g_i(t=0)$.

We now present the nonlinear characteristic method, which avoids these problems. One loads the particles with the equilibrium distribution $g(t=0) = f_0$ (as above, g is the particle distribution) in the same manner as in the usual particle simulation. Then we

assume $g = f = f_0 + \delta f$ throughout the simulation. Since $\frac{1}{f} = \frac{1}{f_0}\left(1 - \frac{\delta f}{f}\right)$, from Eq. (12), we arrive at

$$\dot{w}_i = -\left[\left(\mathbf{v}_E \cdot \frac{\nabla f_0}{f_0} + \frac{q}{m} E_{\|} \frac{\partial_{v_\|} f_0}{f_0}\right)\left(1 - \frac{\delta f}{f}\right)\right]_{\mathbf{x}=\mathbf{x}_i, v_\| = v_{\|i}, \mu=\mu_i, t}. \tag{13}$$

To determine $\delta f/f$ in Eq. (13), we note the following

$$\delta f \approx \frac{\delta f}{f} \sum_i \delta(\mathbf{R} - \mathbf{R}_i)\delta(v_\| - v_{\|i})\delta(\mu - \mu_i) \tag{14}$$

$$= \sum_i \delta(\mathbf{R} - \mathbf{R}_i)\delta(v_\| - v_{\|i})\delta(\mu - \mu_i)\left[\frac{\delta f}{f}\right]_{\mathbf{x}=\mathbf{x}_i, v_\| = v_{\|i}, \mu=\mu_i, t}. \tag{15}$$

The "approximately equal to" sign was used again because we assumed that f and δf were smooth functions, as was done in Eq. (11). From Eqs. (7) and (15) we see that $w_i = [\delta f/f]_i$, and, hence, we can substitute this into Eq. (13) to obtain

$$\dot{w}_i = -(1 - w_i)\left[\left(\mathbf{v}_E \cdot \frac{\nabla f_0}{f_0} + \frac{q}{m} E_{\|} \frac{\partial_{v_\|} f_0}{f_0}\right)\right]_{\mathbf{x}=\mathbf{x}_i, v_\| = v_{\|i}, \mu=\mu_i, t}. \tag{16}$$

Equation (16) along with Eqs. (4), (5) and (7) are the crux of the new nonlinear characteristic method [as usual, one uses Eqs. (2) and (3) to complete the loop]. Besides the nonlinearities appearing as perturbations to the zeroth-order trajectories [$E_\|$ and $\mathbf{v}_E$ in Eqs. (4) and (5)], there is the additional factor $(1 - w_i)$ in the evolution of the equation for the weights in Eq. (16). This factor, which is essential to the nonlinear physics and the conservation properties of the simulation plasma, describes the difference between $f_0(t = 0)$ and $f_0(t)$, as indicated by Eq. (12).

Let us now discuss the conservation of the total particle number, momentum and total energy associated with the new nonlinear weighting scheme. First, we examine the change in "the number of particles" by taking the zeroth velocity moment of Eq. (1). Using Eq. (7) and assuming that the sum of the w_i's is nearly zero initially, we then obtain

$$\sum_i w_i(t) = 0. \tag{17}$$

The momentum conservation can be derived by taking the first velocity moment of Eq. (1),

$$\partial_t \left\{\int v_\| \delta f d\mathbf{R} d\mu dv_\|\right\} - \frac{q}{m}\left\{\int n E_\| d\mathbf{R}\right\} = 0, \tag{18}$$

which, along with Eqs. (2) and (7), then gives

$$\sum_{\alpha} m_{\alpha} \sum_{i} v_{\|\alpha i} w_{\alpha i} = 0, \tag{19}$$

where n is given by Eq. (3) and α denotes species. To calculate the change in energy,[4] we take the second velocity moments of Eq. (1) for both the ions and the electrons and substituting them into Eq. (2). Again, if we take the particle weights and field to be zero at $t = 0$, then the simulation should conserve energy, i.e.,

$$\sum_{\alpha} \frac{m_{\alpha}}{2} \sum_{i} (\mu_{\alpha i} + v_{\|\alpha i}^2) w_{\alpha i} + \left(\frac{\rho_s}{\lambda_D}\right)^2 \frac{1}{8\pi} \int |\nabla_{\perp} \phi|^2 d\mathbf{R} = 0. \tag{20}$$

We expect Eqs. (17)-(20) to hold for a simulation plasma in the limit of large number of particles and fine space and time resolution. In the next section, we will examine the validity of these conservation properties in a simulation using a finite number of particles. This is an important exercise which serves as a test for both the formal correctness as well as the practicality of the proposed scheme. In other words, we want to examine the scheme to see if it is a useful alternative to conventional particle methods.

III. One Dimensional Drift Wave Simulation

We now present simulation results using the new method checking linear and nonlinear physics as well as the conservation properties. For simplicity, a one dimensional drift wave problem is chosen as an example here. In this one dimensional model the $E \times B$ nonlinearity is not present, so the $E_{\|} \partial_{v_{\|}} \delta f$ nonlinearity is the only mechanism for saturation. This is the term which has been neglected in the previous scheme[1] on the assumption that, in the more realistic two and three dimensional geometries, it is the the $E \times B$ nonlinearity which is the dominant saturation mechanism. However, as suggested in Ref. 10 and 11, the $E_{\|} \partial_{v_{\|}} \delta f$ nonlinearity may be relevant in determining the steady-state transport for gradient-driven microinstabilities.

In this problem the one spatial dimension y is perpendicular to the spatial gradients, which are in the x direction, and is almost perpendicular to the magnetic field, $\hat{\mathbf{b}} = \hat{\mathbf{z}} + \theta \hat{\mathbf{y}}$.

Here, both x and z are ignorable coordinates for the perturbation quantities. The one dimensional version of Eq. (1) for both the ions and the electrons is

$$\partial_t \delta f + \theta v_{||} \partial_y \delta f - \alpha \theta \partial_y \phi \partial_{v_{||}} \delta f = -\kappa \partial_y \phi f_0 + \alpha \theta \partial_y \phi \frac{v_{||}^2}{v_t^2} f_0, \tag{21}$$

where $\alpha = (1, -m_i/m_e)$ for the ions and the electrons, respectively; and we use the dimensionless gyrokinetic units of $y/\rho_s \rightarrow y$, $\Omega_i t \rightarrow t$, $v_{||}/c_s \rightarrow v_{||}$, and $e\phi/T_e \rightarrow \phi$. For this problem, we use $\kappa = -\partial_x ln n_0$ and have assumed a Maxwellian equilibrium. The gyrokinetic Poisson equation or the "quasineutrality" condition in one dimension is

$$\partial_{yy} \phi + \delta n_i = \delta n_e. \tag{22}$$

We solve these equations with a one dimensional gyrokinetic simulation using the new method explained in Sec. 2. In addition, a quiet start technique employing Fibonacci numbers[8] has been used. In order to further minimize the noise, we have also used a cutoff scheme[1] of

$$w_i = \phi(x_i) \tag{23}$$

for the fast particle with $v_{||i} \gg \omega/k_{||}$. ϕ_m is initially perturbed, where m is the Fourier harmonics of interest. Since our purpose is to study the nonlinear electron dynamics, we have also linearized the ion motion in the simulation by discarding the $\partial_{v_{||}} \delta f$ term in Eq. (21), which is accomplished in the simulation by letting $v_{||} = 0$ for Eq. (4) and dropping the $(1 - w_i)$ correction in Eq. (16).

The first run shown has the following parameters in the gyrokinetic units: $T_e/T_i = 1$, $m_i/m_e = 1837$, the magnetic field tilt $\theta = 0.01$, the particle size is one $(= \rho_s)$, the timestep is $\Delta t = 1$, $\kappa_n = 0.2$, the system size is $L = 16\Delta x$, the grid size is $\Delta x = 0.5$, and the total number of particles is $N_{tot} = f_{16} = 987$, where f_{16} denotes the sixteenth Fibonacci number. With this choice of parameters the dominant unstable mode is the $n = 1$ harmonic or $k = 2\pi/L \simeq 0.8$ mode. Figure 1(a) shows the the time evolution of the electrostatic potential for $n = 1$ Fourier mode. The real part is the solid line and the imaginary part is the dashed line. The mode frequency averaged over both the linear and nonlinear parts of the evolution is $\omega \simeq 0.075$. Figure 1(b) gives the logarithmic change of the

amplitude as a function of time for this mode. A clean linear growth followed by a sudden nonlinear saturation is clearly visible. The measured linear growth rate is $\gamma \simeq 0.012$, and the saturation amplitude is $\phi \simeq 1.1\%$. Figure 2(a) shows the spatially averaged perturbation $\delta f_{e0}(\equiv \langle \delta f \rangle)$ at $t = 500$ and gives the resonant point at $v_{||} = 0.2 v_{te}$. Integrating δf_{e0} in $v_{||}$, we obtain $\mid \sum_i w_i / N_{tot} \mid \simeq 1.3 x 10^{-4}$ at $t = 500$; thus, the particle conservation deviates from Eq. (17). This discrepancy, which increases by a factor of 2.5 at the end of the run, has no effect on the instability, it is however, a measure of accuracy of the simulation. Another interesting aspect of the simulation is that, while we are solving Eq. (21), we also follow the evolution of the equation $\dot{f} = 0$ with the same set of equations of motion and

$$f(y, v_{||}, t) = \sum_{i=1}^{N} S(y - y_i) \delta(v_{||} - v_{||i}). \tag{24}$$

The total distribution function f at $t = 500$ is shown in Fig. 2(b). Its jaggedness, compounded by the fact that δf_{e0} is not at all discernible, would make it impossible to use this information for conservation property diagnostics, let alone for the field solve.

Because of the use of the linear ion response, the momentum conservation given by Eq. (18) cannot be satisfied in the simulation. However, we can use Eq. (19) to check a similar property. In the one dimensional system, it becomes[12]

$$\frac{d}{dt} \langle \int v_{||} \delta f_e dv_{||} \rangle + \frac{m_i}{m_e} \theta \langle \Gamma_e \rangle = 0, \tag{25}$$

where $\Gamma_e \equiv -\partial_y \varphi n_e$ is the particle flux, and $\langle \cdots \rangle$ denotes spatial average. Hence, we obtain a relationship between the rate of change of the momentum and the particle flux in the simulation, which is plotted in Fig. 3(a). Here, a frequency filter has been used to smooth the data for dp_e/dt and the normalization constant n_0 is the average number density. Apparently, numerical noise for the flux is quite substantial and, again, there is a discrepancy of $O(10^{-4})$ between these two quantities. From Eq. (20), the energy conservation becomes,

$$\langle \int \delta f v_{||}^2 dv_{||} \rangle / n_0 v_t e^2 + \langle \mid \partial_y \phi \mid^2 \rangle = 0. \tag{26}$$

This is shown in Fig. 3(b). Again, the results are quite noisy and the difference between the kinetic energy and the field energy is also of $O(10^{-4})$. However, considering the small

number of particles used in the simulation, these results are actually quite good. We remind the reader that this was accomplished through the use of: 1) nonlinear weighting scheme, 2) the quiet start technique, and 3) the nonrandom initial perturbation.

Nevertheless, the errors in the conservation properties after nonlinear saturation is troublesome, since our ultimate goal is to use the scheme to study long-time steady-state phenomena. To improve upon these results, we have carried out a series of runs and found that a substantial increase in numerical accuracy is needed. To illustrate this point, we now present a run with $\Delta t = 0.2$, $N_{tot} = 46,368$ particles on a 64-grid system using a particle size of $\rho_s/2$. All the other parameters remain the same. Figures 4(a) and (b) show the mode history. Comparing with the previous case, the mode frequency (averaged over both the linear and nonlinear parts of the evolution) increases slightly to $\omega \simeq 0.088$, and the saturation level decreases slightly to $\phi \simeq 1\%$, while the growth rate remains the same at $\gamma \simeq 0.012$. One important difference is that the numerical (including noise) errors remain small in the nonlinear stage when the particles are trapped and executing bounce motion. This characteristic is clearly manifested in the diagnostics for the perturbed distribution function δf_{e0} and f in Figs 5(a) and (b). However, for the perturbed distribution, which is also measured at $t = 500$, the asymmetry in the velocity space still remains, and the corresponding discrepancy for the total particle number, $\mid \sum_i w_i/N_{tot} \mid$, averages to about 1.35×10^{-4}, which is similar to the previous course simulation. However, the overall smoothness of the distributions in Figs. 5(a) and (b) come from the increase in numerical accuracy. Interestingly, even with this type of accuracy, the perturbation of δf_{e0} is still not quite discernible in the total f diagnostic Fig. 5(b). This is because the perturbation is only a factor of two above the thermal fluctuation level of $\phi = 1/\sqrt{N_{tot}}k \simeq 0.6\%$.[4] Thus, following from Ref. 1, one can surmise that a total f simulation, even with this many particles, would not give as clean a result as the new scheme. This point cannot be verified, however, because there is no available scheme to solve the equation of the form, $\dot{f} = -\kappa \partial_y \phi f_0$. The corresponding flux and energy diagnostics for this case are shown in Figs. 6(a) and (b). As we can see, the conservation of both these quantities are near perfect. The implication here seems to be that one still has to use a very large number of particles with enough spatial and time

resolution to obtain reasonable conservation properties. On the other hand, a conventional particle simulation would need even more. However, if one is only interested in linear growth and nonlinear saturation, the present scheme represents a substantial savings in computing resources.

IV. Nonlinear Saturation

The nonlinear saturation of the most unstable modes (e.g., $n = \pm 1$ in the simulation results presented above) is due to the parallel velocity nonlinearity and is not caused by $E \times B$ advection. It is commonly assumed that the the $E \times B$ nonlinearity, which is absent in the simple one dimensional model, is the dominant nonlinearity for the saturation of the drift waves in the (more realistic) higher dimensional models. However, the parallel nonlinearity does play a role in the saturation as was shown in Ref. 11. The simulation results in Sec. 3 indicate that the saturation level is comparable to the $E \times B$ saturation level $e|\phi|/T_e \sim \gamma/(k_\perp^2 c_s \rho_s)$ (assuming $k_x \sim k_y$),[11] and is much lower then $e|\phi|/T_e \sim \frac{1}{4}(k_\perp \rho_s)^2$, as predicted by Sagdeev and Galeev.[5] Also, in a tokamak geometry, drift type modes are elongated in the radial direction ($k_r \ll k_\theta$), at least in the linear phase, which should reduce the effect of the $E \times B$ on saturation.[13–15] In addition, the parallel nonlinearity may be important in determining the steady-state transport caused by microturbulence,[16] which will not be discussed here. The one dimensional model allows us to isolate the parallel nonlinearity and study the associated physics.

In this section, we consider a simple case of three-wave coupling between the two fastest growing modes ($n = \pm 1$) and δf_0 for the electrons. The saturation takes place when the electron electron distribution is steepened at the resonance point $k_\parallel v_\parallel = \omega$. The saturation amplitude of the potential due to the $E_\parallel \partial_{v_\parallel} \delta f$ nonlinearity is calculated using a quasilinear estimate which is similar to the calculation for saturation of drift waves due to the $E \times B$ nonlinearity given in Ref. 11. In the following, we use the subscript "1" to label the fastest growing mode and its complex conjugate with $k = 2\pi n/L$, where L is the system length, and n is the Fourier mode number. [Note that $\delta f_1(k) = \delta f_1^*(-k)$]. The governing drift-kinetic

electron equations are

$$\partial_t \delta f_1 + k_{||} v_{||} \partial_y \delta f_1 + i(\omega_* - k_{||} v_{||}) f_0 + i \frac{m_i}{m_e} k_{||} \phi_1 \partial_{v_{||}} \delta f_0 = 0, \quad (27)$$

$$\partial_t \delta f_0 - 2 \frac{m_i}{m_e} k_{||} \phi_1 \partial_{v_{||}} Im(\phi_1 \delta f_1^*) = 0, \quad (28)$$

where $\omega_* = \kappa k$ (in the gyrokinetic units), f_0 is the background Maxewellian and δf_0 is the nonlinear change of the background due to mode coupling. The perturbed electron density is $\delta n_{e1} = \int \delta f_1 dv_{||}$. For the ions, we assume a fluid response since $|\omega/k_{||}| \gg v_{ti}$, and the continuity equation for ion density becomes

$$\partial_t \delta n_{i1} + i\omega_* \delta n_{i1} = 0. \quad (29)$$

Equations (22) and (27)-(29) could be solved using the Vlasov (Eulerian) simulation and should give the same results as the particle simulation in the previous section. However, to obtain an analytic estimate, we assume the dependence of $e^{-i\omega t}$ for δf_1, n_{i1}, and ϕ_1, where $\omega = \omega_r + i\gamma$ and also $|\omega_r/\gamma| \gg 1$. The perturbation can then be expressed as

$$\delta f_1 = \left\{ f_0 - \frac{(\omega_* - \omega_r)}{(k_{||} v_{||} - \omega)} f_0 - \frac{m_i}{m_e} \frac{k_{||}}{(k_{||} v_{||} - \omega)} \partial_{v_{||}} \delta f_0 \right\} \phi_1. \quad (30)$$

Assuming γ small, we can use the following relation

$$\frac{1}{(k_{||} v_{||} - \omega)} = \frac{k_{||} v_{||} - \omega_r + i\gamma}{|k_{||} v_{||} - \omega|^2} \approx i\pi \delta(k_{||} v_{||} - \omega_r), \quad (31)$$

to obtain the electron density response as

$$\delta n_{e1} = \int_{-\infty}^{+\infty} \delta f_1 dv_{||} = \left\{ 1 - i\sqrt{\frac{\pi}{2}} \frac{1}{k_{||} v_{te}} (\omega_* - \omega_r) - \frac{m_i}{m_e} \int_{-\infty}^{+\infty} \frac{k_{||}}{(k_{||} v_{||} - \omega)} \partial_{v_{||}} \delta f_0 dv_{||} \right\} \phi_1. \quad (32)$$

From which we arrive at the following nonlinear dispersion relation

$$1 + k^2 - \frac{\omega_*}{\omega} - i\sqrt{\frac{\pi}{2}} \frac{1}{k_{||} v_{te}} (\omega_* - \omega_r) - \frac{m_i}{m_e} \int_{-\infty}^{+\infty} \frac{k_{||}}{(k_{||} v_{||} - \omega)} \partial_{v_{||}} \delta f_0 dv_{||} = 0. \quad (33)$$

Neglecting the nonlinear term (last term on the right), we obtain the familiar linear results[11]

$$\omega_r = \omega_l \equiv \frac{\omega_*}{1 + k^2}, \quad (34)$$

$$\gamma = \gamma_l \equiv \sqrt{\frac{\pi}{2}} \frac{1}{(k_{||} v_{te})} \frac{\omega_l}{(1 + k^2)} (\omega_* - \omega_l). \quad (35)$$

The predicted linear frequency and growth rate for the simulation are: $\omega_l = 0.0976$ and $\gamma_l = 0.0134$, which are very close to the results shown in Figs. 1 and 4. From the linear response for δf_1, the nonlinear response of the background can be estimated as

$$\delta f_0 = \pi \frac{m_i}{m_e} \frac{k_\parallel}{\gamma} |\phi_1|^2 (\omega_* - \omega_l) \partial_{v_\parallel} \left\{ \delta(k_\parallel v_\parallel - \omega_l) f_0(v_\parallel) \right\}. \tag{36}$$

Substituting Eq. (36) into Eq. (33), we obtain the nonlinear dispersion relation in terms of the amplitude of ϕ_1

$$1 + k^2 - \frac{\omega_*}{\omega} - i\sqrt{\frac{\pi}{2}} \frac{1}{k_\parallel v_{te}} (\omega_* - \omega_l) \left\{ 1 - 2\frac{k_\parallel^4}{\gamma_l^4} \left(\frac{m_i}{m_e} \right)^2 |\phi_1|^2 \right\} = 0. \tag{37}$$

From this equation, again assuming $|\gamma/\omega| \ll 1$, we obtain the same real frequency $\omega_r = \omega_l$, but the the quasilinear value for the growth rate becomes

$$\gamma = \gamma_l \left\{ 1 - 2\frac{(k_\parallel v_{te})^4}{\gamma_l^4} |\phi_1|^2 \right\}. \tag{38}$$

At saturation $\gamma = 0$, the saturation level of the potential can be expressed as

$$|\phi_1| = \frac{1}{\sqrt{2}} \frac{\gamma_l^2}{(k_\parallel v_{te})^2}. \tag{39}$$

Using the simulation parameters of $k_\parallel = \theta 2\pi / L = 0.00785$, $m_i/m_e = 1837$, and $\gamma_l = 0.0134$, the predicted saturation amplitude is $|\phi_1| = 0.11\%$, which is an order of magnitude smaller than the level obtained from the simulation results shown in Figs. 1 and 4. Thus, the effect of parallel nonlinearity on the saturation is overly estimated by the above approximation.

Next, to improve on this first estimate, we use the original form of the resonant denominator, Eq. (31), and also use the full nonlinear δf_1 to calculate δf_0, i.e.,

$$\delta f_0 = \frac{m_i}{m_e} k_\parallel |\phi_1|^2 (\omega_* - \omega_r) \partial_{v_\parallel} \left\{ \frac{f_0}{|k_\parallel v_\parallel - \omega_r|^2} \left[1 + \frac{m_i}{m_e} \frac{k_\parallel}{(\omega_* - \omega_l)} \frac{\partial_{v_\parallel} \delta f_0}{f_0} \right] \right\}, \tag{40}$$

If the quasilinear approximation is valid, this second order ordinary differential equation could be solved to obtain δf_0, which in turn could be used in Eq. (33) to obtain an accurate prediction of the saturation level. The extra term included in Eq. (40) accounts for the effect of parallel trapping on saturation. To obtain an simpler estimate, we begin by using the δ-function relation, Eq. (31), in Eq. (40) to obtain

$$\delta f_0 = (1 - \alpha)\, f_0|_{v_\parallel = \omega_r / k_\parallel} \frac{m_i}{m_e} k_\parallel |\phi_1|^2 (\omega_* - \omega_l) \partial_{v_\parallel} |k_\parallel v_\parallel - \omega|^{-2}, \tag{41}$$

where $\alpha = -\frac{m_i}{m_e}\frac{k_\parallel}{(\omega_* - \omega_l)}\left.\frac{\partial_{v_\parallel}\delta f_0}{f_0}\right|_{v_\parallel=\omega_r/k_\parallel}$. Then, substituting Eq. (41) in Eq. (33), assuming $|\omega/k_\parallel| \ll v_{te}$, and integrating, we obtain the following relation for the saturation amplitude

$$|\phi_1| = \frac{2}{\sqrt{1-\alpha}}\frac{\gamma_l^2}{(k_\parallel v_{te})^2}. \tag{42}$$

Assuming a linear response for δf_1 as was done in deriving Eq. (39), so that $\alpha = 0$, we obtain $|\phi_1| = 0.32\%$, which is in better agreement with the simulation results than Eq. (39), but it still too low.

An estimate of α can be made by taking the derivative of Eq. (40) with respect to $v_\parallel$, and evaluate at $v_\parallel = \omega_r/k_\parallel$ to obtain

$$\begin{aligned}\left.\partial_{v_\parallel}\delta f_0\right|_{v_\parallel=\omega_r/k_\parallel} &= \frac{m_i}{m_e}k_\parallel|\phi_1|^2\left\{(\omega_* - \omega_l)f_0(v_\parallel)\partial_{v_\parallel}^2|k_\parallel v_\parallel - \omega_r|^{-2}\right. \\ &\left. + \frac{m_i}{m_e}k_\parallel\left[\left(\partial_{v_\parallel}\delta f_0\right)\partial_{v_\parallel}^2 + \left(\partial_{v_\parallel}^3\delta f_0\right)\right]|k_\parallel v_\parallel - \omega_r|^{-2}\right\}_{v_\parallel=\omega_r/k_\parallel},\end{aligned} \tag{43}$$

where we have neglected derivatives of $f_0(v_\parallel)$ because it is slowly varying compared to $|k_\parallel v_\parallel - \omega_r|^{-2}$. We have also neglected $\partial_{v_\parallel}^2\delta f_0$ terms, by assuming δf_0 has the following form

$$\delta f_0 = C(t)v_\parallel \exp\left[-\frac{1}{2}\frac{v_\parallel^2}{\Delta v_\parallel^2(t)}\right], \tag{44}$$

where C and $\Delta v_\parallel$ are independent of $v_\parallel$, and $\Delta v_\parallel \approx \sqrt{2|\phi_1(t)|\frac{m_i}{m_e}}$ is the width of the trapping region [see Fig. 5(a)]. From Eq. (44), one can show that $\left.\partial_{v_\parallel}^2\delta f_0\right|_{v_\parallel=\omega_r/k_\parallel} \simeq 0$. In addition, we can use the relationship of $\partial_{v_\parallel}^3\delta f_0 \simeq -\frac{3}{\Delta v_\parallel^2}\partial_{v_\parallel}\delta f_0$, to obtain an equation for α, i.e.,

$$\alpha = \frac{2z^2}{2z^2 + \frac{3}{2}z + 1}, \tag{45}$$

where $z = \frac{(v_{te}k_\parallel)^2}{\gamma_l^2}|\phi_1|$. We can now substitute this approximate value of α into Eq. (42) to obtain the following cubic equation

$$\frac{3}{8}z^3 - \frac{7}{4}z^2 - \frac{3}{2}z - 1 = 0. \tag{46}$$

Solving Eq. (46), we find

$$|\phi_1| = 5.48\frac{\gamma_l^2}{(k_\parallel v_{te})^2}, \tag{47}$$

along with two spurious complex roots with negative real parts. Equation (47) yields $|\phi_1| = 0.87\%$ for our simulation parameters, which is in good agreement with the the results shown in Figs. 1 and 4. We have also tried an iterative solution using the linear value of δf_1 to obtain the first iteration δf_0^1, then using $\partial_{v_\parallel} \delta f_0^1$ in Eq. (40) to predict δf_0^2, etc. However, this procedure did not converge.

V. General Nonlinear Characteristic Method

In this Section we extend the nonlinear scheme previously discussed for the electrostatic slab in Sec. 2 to the toroidal finite-β gyrokinetic equations. We begin, as before, by writing $f(\mathbf{z},t) = f_0(\mathbf{z}) + \delta f(\mathbf{z},t)$, where $\mathbf{z} = (\mathbf{R}, v_\parallel, \mu)$, and $f_0(\mathbf{z})$ is an equilibrium distribution which satisfies $\dot{\mathbf{z}}_0 \cdot \partial_{\mathbf{z}} f_0(\mathbf{z}) = 0$. Using the electromagnetic gyrokinetic equations with a nonuniform equilibrium B-field[17-20] and writing $\dot{\mathbf{z}}$ as an equilibrium and perturbed part, $\dot{\mathbf{z}} = \dot{\mathbf{z}}_0 + \dot{\mathbf{z}}_1$, the equation for δf is

$$\partial_t (B^* \delta f) + \partial_{\mathbf{z}} \cdot (\dot{\mathbf{z}} B^* \delta f) = -\dot{\mathbf{z}}^1 \cdot \partial_{\mathbf{z}} f_0. \tag{48}$$

where μ is time independent, and the equilibrium and perturbed trajectories are evolved using

$$\dot{\mathbf{R}}^0 = \frac{1}{B^*} \left\{ v_\parallel \mathbf{B}^{*0} + \frac{c}{e} \hat{\mathbf{b}} \times \mu \nabla B^0 \right\}, \tag{49}$$

$$\dot{v}_\parallel{}^0 = -\frac{1}{B^*} \left\{ \mathbf{B}^{*0} \cdot \frac{\mu}{m} \nabla B^0 \right\}, \tag{50}$$

$$\dot{\mathbf{R}}^1 = \frac{1}{B^*} \left\{ v_\parallel \delta \mathbf{B}_\perp + \frac{c}{e} \hat{\mathbf{b}} \times \mu \nabla \delta B_\parallel + c \hat{\mathbf{b}} \times \nabla \delta \phi \right\}, \tag{51}$$

$$\dot{v}_\parallel{}^1 = -\frac{1}{B^*} \left\{ \mathbf{B}^{*0} \cdot \left(\frac{\mu}{m} \nabla \delta B_\parallel + \frac{e}{m} \nabla \delta \phi + \frac{e}{mc} \partial_t \delta A_\parallel \hat{\mathbf{b}} \right) + \delta \mathbf{B}_\perp \cdot \frac{\mu}{m} \nabla B^0 \right\}, \tag{52}$$

where $\mathbf{B}^* = \mathbf{B}^0 + \delta \mathbf{B}_\perp + \frac{mc}{e} u \nabla \times \hat{\mathbf{b}}$, $B^* = \hat{\mathbf{b}} \cdot \mathbf{B}^*$, and $\mathbf{B}^{*0} = \mathbf{B}^0 + \frac{mc}{e} u \nabla \times \hat{\mathbf{b}}$.

The characteristics (or particles) follow the full nonlinear trajectories $\mathbf{z} = \mathbf{z}^0 + \mathbf{z}^1$, and δf is represented by

$$B^* \delta f(\mathbf{z},t) = \sum_i w_i \delta(\mathbf{z} - \mathbf{z}_i). \tag{53}$$

We define g as a smooth distribution function representing the particle distribution (g does not necessarily have to be equal to the physical distribution function f at this point)

$$B^* g(\mathbf{z}, t) \approx \sum_i \delta(\mathbf{z} - \mathbf{z}_i). \tag{54}$$

Substituting Eq. (53) into Eq. (48) and using Eq. (54), we obtain

$$\dot{w}_i = -\left[\dot{\mathbf{z}}^1 \cdot \frac{\partial_{\mathbf{z}} f_0}{g(\mathbf{z}, t)}\right]_{\mathbf{z}=\mathbf{z}_i,t}. \tag{55}$$

which is just the generalization of Eq. (12). If , as before, we take $g = f = f_0 + \delta f$ we obtain

$$\dot{w}_i = -(1 - w_i)\left[\dot{\mathbf{z}}^1 \cdot \frac{\partial_{\mathbf{z}} f_0}{f_0}\right]_{\mathbf{z}=\mathbf{z}_i,t}. \tag{56}$$

This evolution equation for w_i along with the equations for the nonlinear trajectories Eqs. (49)-(52), is the more general version of the new method presented in Sec. 2.

VI. Discussion

We have developed a new nonlinear characteristic method which retains all nonlinearities in a consistent way. This, however, does not preclude the possibility of neglecting various nonlinear terms if they are physically unimportant. In fact various terms can easily be "turned on and off" to test their physical effect. We also see no immediate difficulties in applying this method to other Vlasov-Maxwell systems where the derivatives of the initial distribution are known and finite. For a strong instability, where the perturbations become large $\delta f/f \approx 1$, noise properties revert back to those of a conventional particle simulation. However, in such a case the linear phase would be much more accurately resolved. At best, the new method captures the physics of conventional particle schemes with improved statistical properties. At worst, the scheme behaves linearly (with very low noise properties) for small perturbations, and fully nonlinear (with associated thermal noise) for large perturbations, and consistently makes the transition between the two extremes. We were able to obtain good energy conservation. However, compared to the number needed to capture the relevant physics of the drift wave model, a very large number of particles were required. The saturated electrostatic energy and associated change in electron kinetic

energy is only 1.0% of the total electron thermal energy for the choice of parameters in Sec. 3. As such, it is not surprising that a relatively large number of particles, small timestep and fine grid where required to resolve this small change in kinetic energy (1.0% of the total).

This one dimensional drift wave model permits us to isolate $E_{||}\partial_{v_{||}}\delta f$ nonlinearity and the associated nonlinear physics. Mode coupling theory was used to obtain a saturation level which is much lower (for our choice of parameters) than the estimate based on the energy balance calculation of Sagdeev and Galeev.[5] Simulation results agree well with our estimate. Because of this new lower saturation amplitude, parallel velocity nonlinearity may play a more important role in microturbulence then previously thought, although past investigations have shown such a tendency.[11] In addition, the existing linear theory for tokamak geometry predicts a ballooning type mode structure which is elongated in the radial direction and, therefore, will reduce the effectiveness of the $E \times B$ nonlinearity for saturation.

Finally, the nonlinear characteristic method was extended to the general electromagnetic gyrokinetic equations. Application of these equations in a three dimensional toroidal simulation is an ongoing effort and will be reported in the future.[15]

Acknowledgments

We thank Dr. Liu Chen, Dr. T.S. Hahm, and Dr. A. Dimits for enlightening discussions. This research was supported in part by an appointment to the U.S. Department of Energy Fusion Energy Postdoctoral Research Program administered by Oak Ridge Associated Universities and by DOE Contract No. DE-AC02-76-CHO-3073.

References

[1] A. Dimits and W. W. Lee, PPPL Report 2718, Oct. 1990 [submitted to J. Comp. Phys.].

[2] T. Tajima and F.W. Perkins, *Proceedings of the Sherwood Fusion Theory Conference*, 2P9 (1983).

[3] M. Kotschenruether, *Proceedings of the 14th International Conference on Numerical Simulation of Plasmas* (Anapolis, MD 1991).

[4] W.W. Lee , J. Comput. Phys. **72**, 243 (1987).

[5] R.Z. Sagdeev and A.A. Galeev, *Nonlinear Plasma Theory*, W.A. Benjamin, Inc., NY (1969).

[6] J.A. Byers, *Proceedings of the Fourth Conference on Numerical Simulation of Plasmas* (NRL,Washington, DC 1970), P. 496.

[7] J.P. Friedberg, R.L. Morse, and C.W. Nielson, *Proceedings of the Third Conference on Numerical Simulation of Plasmas* (Stanford University, CA 1969).

[8] J. Denavit and J.M. Walsh, *Comments in Plasma Phys. Controlled Fusion* **6** 209 (1981).

[9] B.I. Cohen, S.P. Auerbach, J.A. Byers, and H. Weitzner, Phys. Fluids **23**, 2529 (1980).

[10] A. Friedman, R.N. Sudan, and J. Denavit, J. Comput. Phys. **40** 1 (1980).

[11] W.W. Lee, J.A. Krommes, C.R. Oberman, and R.A. Smith, Phys. Fluids **27** 2652 (1984).

[12] W. M. Nevins, Phys. Fluids **22**, 1681 (1979).

[13] S.C. Cowley, R.M. Kulsrud and R. Sudan, Phys. Fluids B **13** 2767 (1991).

[14] Romenelli, L. Chen and S. Briguglio, Phys. Fluids B **3** 2496 (1984).

[15] S.E. Parker and W.W. Lee, *Proceedings of the International Sherwood Fusion Theory Conference*, 1B3 (1992).

[16] W.W. Lee, W.M. Tang, Phys. Fluids, **31** 612 (1988).

[17]T.S. Hahm, W.W. Lee and A. J. Brizard, Phys. Fluids **31** 1940 (1988).

[18]T.S. Hahm, Phys. Fluids **31** 2670 (1988).

[19]A. J. Brizard, J. Plasma Physics **41** 541 (1989).

[20]A.J. Brizard, Ph.D. Thesis, Princeton Univ., Jan. 1990.

Figures

Figure 1 (a) Time history for the real (solid line) and imaginary (dashed line) part of the electrostatic potential for the $n = 1$ drift instability ($k_\perp \rho_i \simeq 0.8$), and (b) the corresponding amplitude evolution for the run with 987 particles on a 16-grid system.

Figure 2 (a) Perturbed distribution $\delta f(k = 0)/f_0(v_\parallel = 0)$, and (b) the total distribution $f/f_0(v_\parallel = 0)$ for the electrons for the 987 particle run at $\Omega_i t = 500$.

Figure 3 (a) Time history for the electron particle flux (solid line), and the time rate of change for the electron parallel momentum (dashed line), and (b) the time evolution for the perturbed electron kinetic energy (solid line), and the field energy (dashed line) for the 987 particle run.

Figure 4 (a) Time history for the real (solid line) and imaginary (dashed line) part of the electrostatic potential for the $m = 1$ drift instability ($k_\perp \rho_i \simeq 0.8$), and (b) the corresponding amplitude evolution for the run with 46368 particles on a 64-grid system.

Figure 5 (a) Perturbed distribution $\delta f(k = 0)/f_0(v_\parallel = 0)$, and (b) the total distribution $f/f_0(v_\parallel = 0)$ for the electrons for the 46368 particle run at $\Omega_i t = 500$.

Figure 6 (a) Time history for the electron particle flux (solid line), and the time rate of change for the electron parallel momentum (dashed line), and (b) the time evolution for the perturbed electron kinetic energy (solid line), and the field energy (dashed line) for the 46368 particle run.

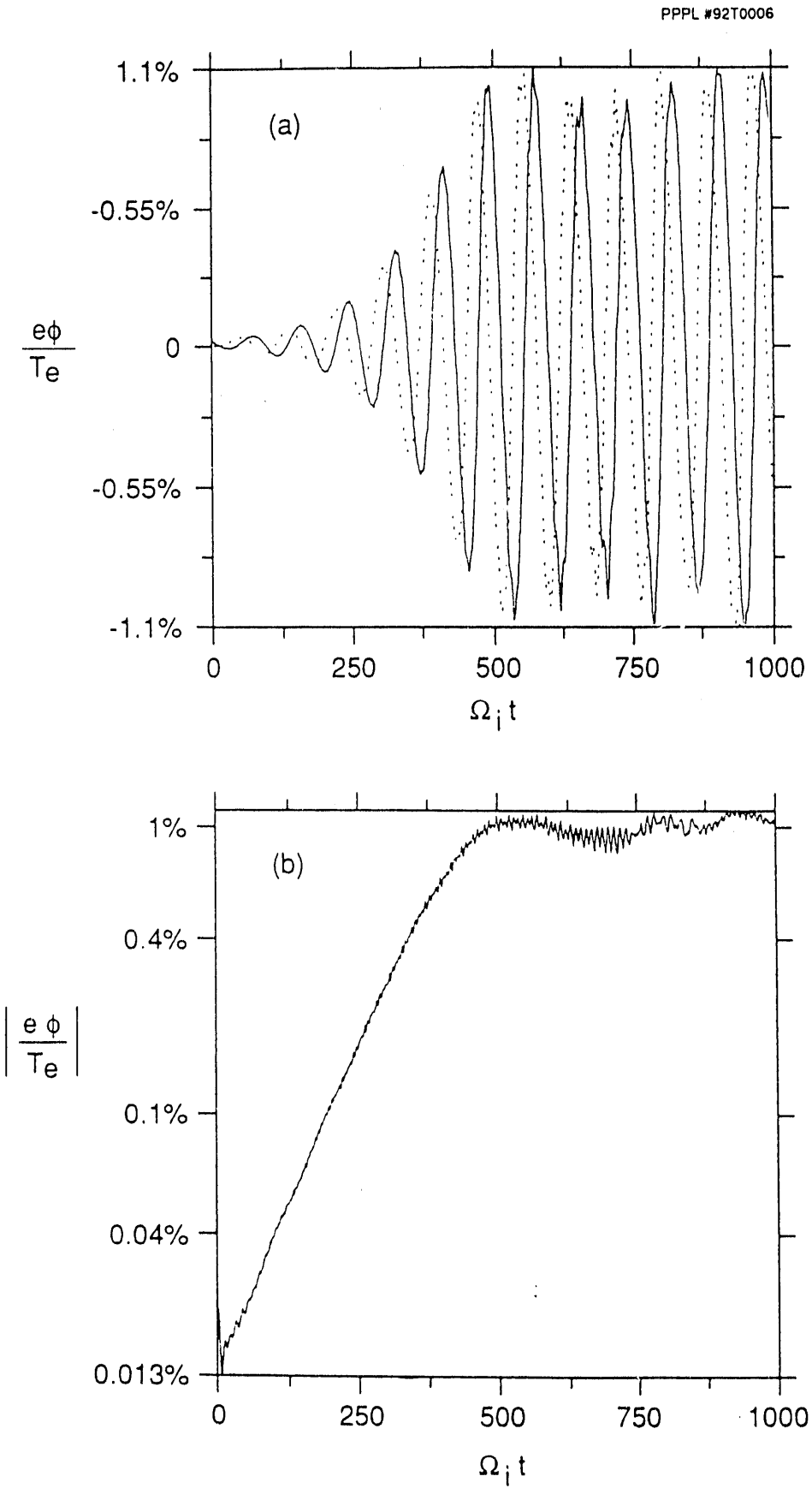
PPPL #92T0006
1.1%
(a)
-0.55%
eφ/Te
0
-0.55%
-1.1%
0
250
500
750
1000
Ωi t
1%
(b)
0.4%
|eφ/Te|
0.1%
0.04%
0.013%
0
250
500
750
1000
Ωi t

Fig. 1

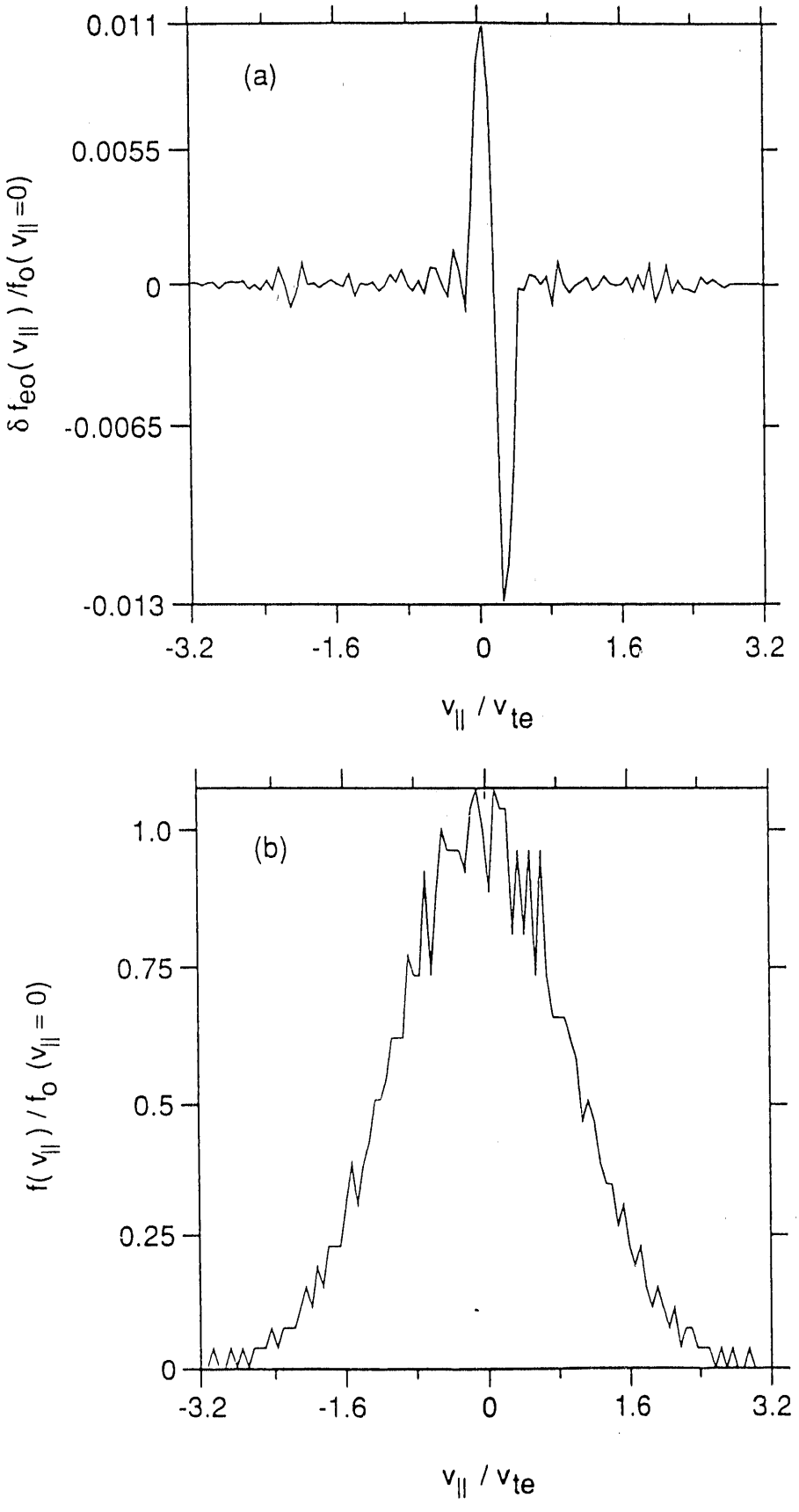
(a)
0.011
0.0055
0
-0.0065
-0.013
-3.2
-1.6
0
1.6
3.2
δ f_eo(v_||) /f_o(v_||=0)
v_|| / v_te
(b)
1.0
0.75
0.5
0.25
0
-3.2
-1.6
0
1.6
3.2
f(v_||) / f_o (v_|| = 0)
v_|| / v_te

Fig. 2

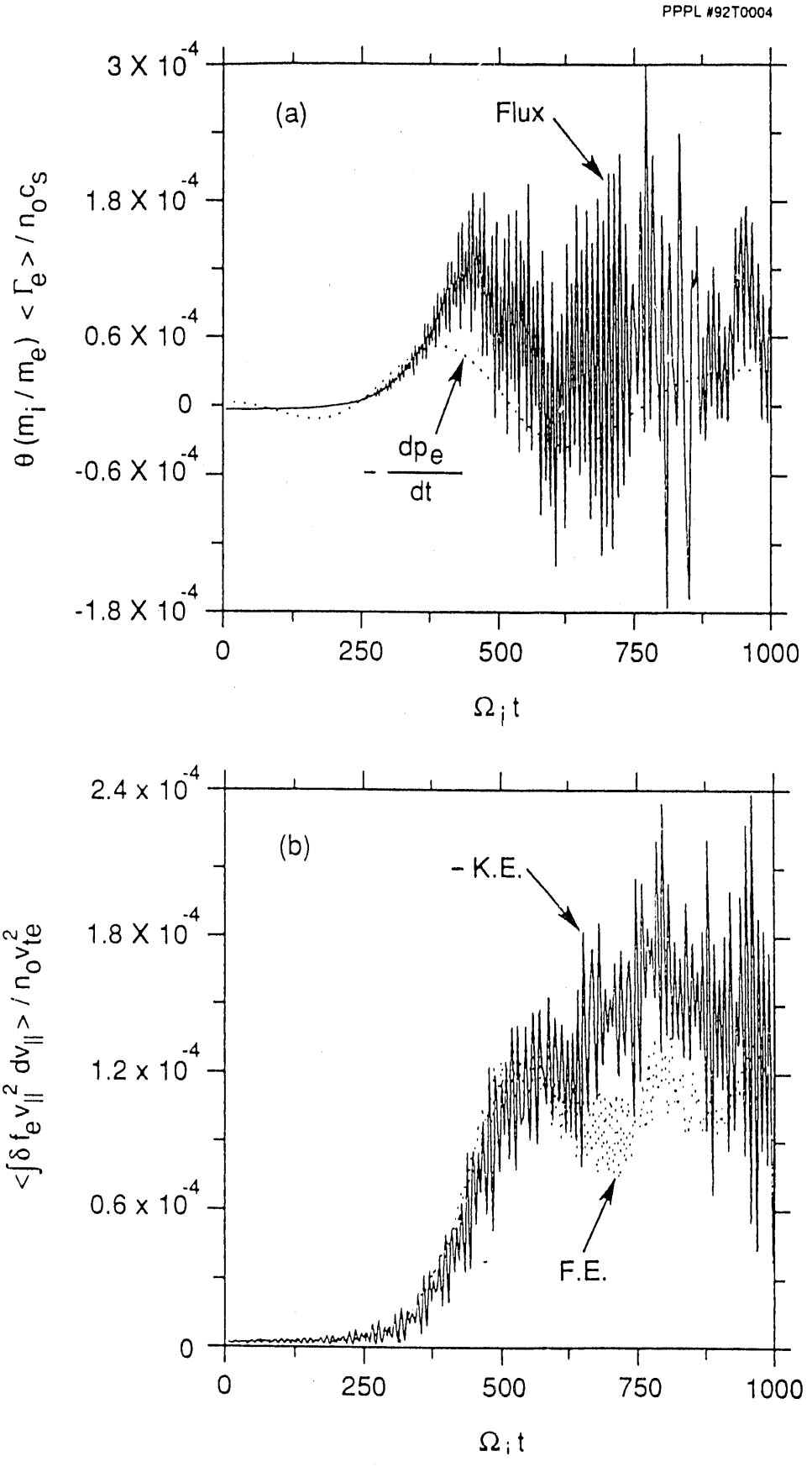
PPPL #92T0004
(a)
Flux
$-\frac{dp_e}{dt}$
$\theta (m_i / m_e) < \Gamma_e > / n_o c_s$
3 X 10^{-4}
1.8 X 10^{-4}
0.6 X 10^{-4}
0
-0.6 X 10^{-4}
-1.8 X 10^{-4}
0
250
500
750
1000
$\Omega_i t$
(b)
- K.E.
F.E.
$<\int \delta f_e v_{||}^2 dv_{||} > / n_o v_{te}^2$
2.4 x 10^{-4}
1.8 X 10^{-4}
1.2 x 10^{-4}
0.6 x 10^{-4}
0
0
250
500
750
1000
$\Omega_i t$

Fig. 3

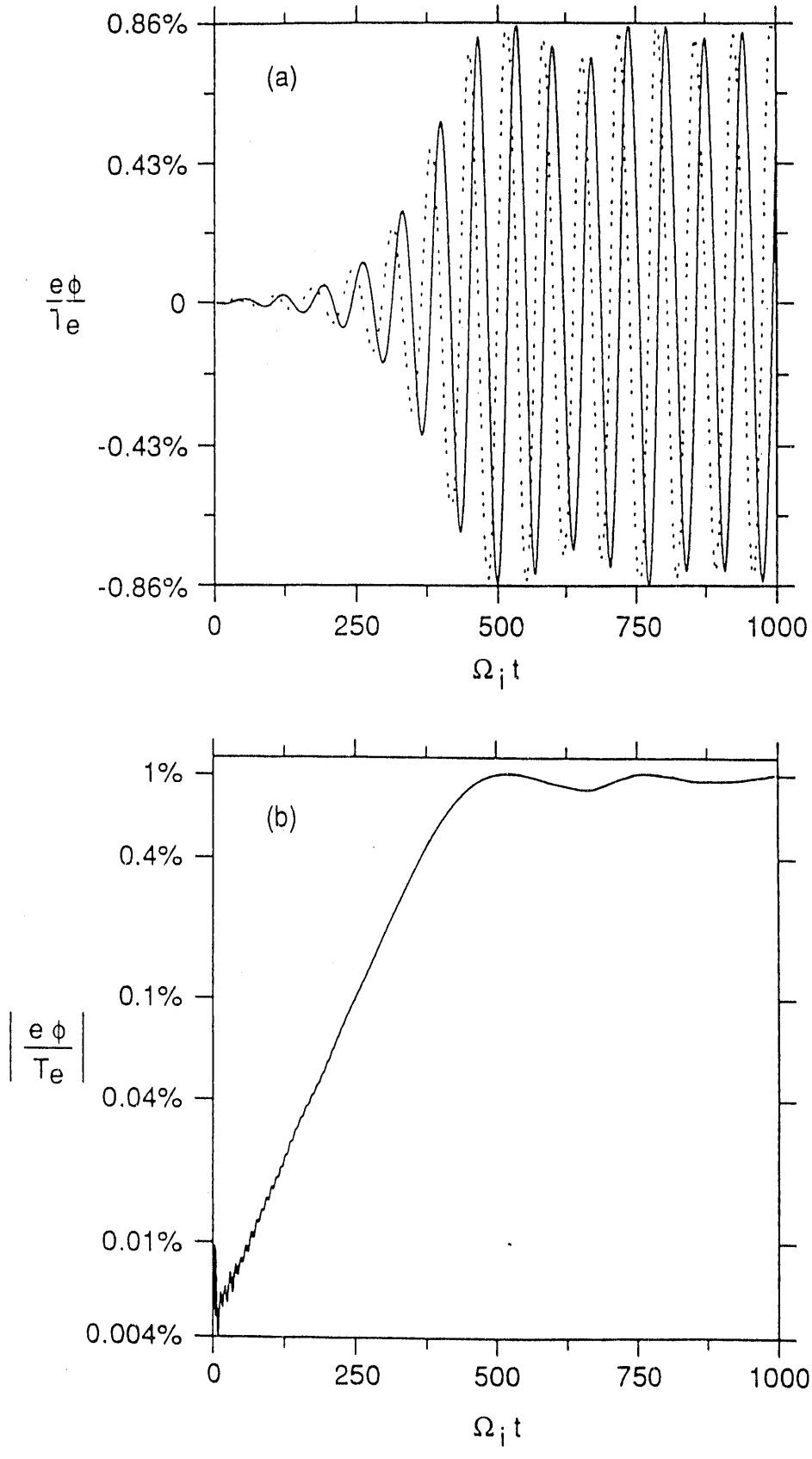
0.86%
0.43%
0
-0.43%
-0.86%
(a)
eφ/Te
0
250
500
750
1000
Ωi t
1%
0.4%
0.1%
0.04%
0.01%
0.004%
(b)
|eφ/Te|
0
250
500
750
1000
Ωi t

Fig. 4

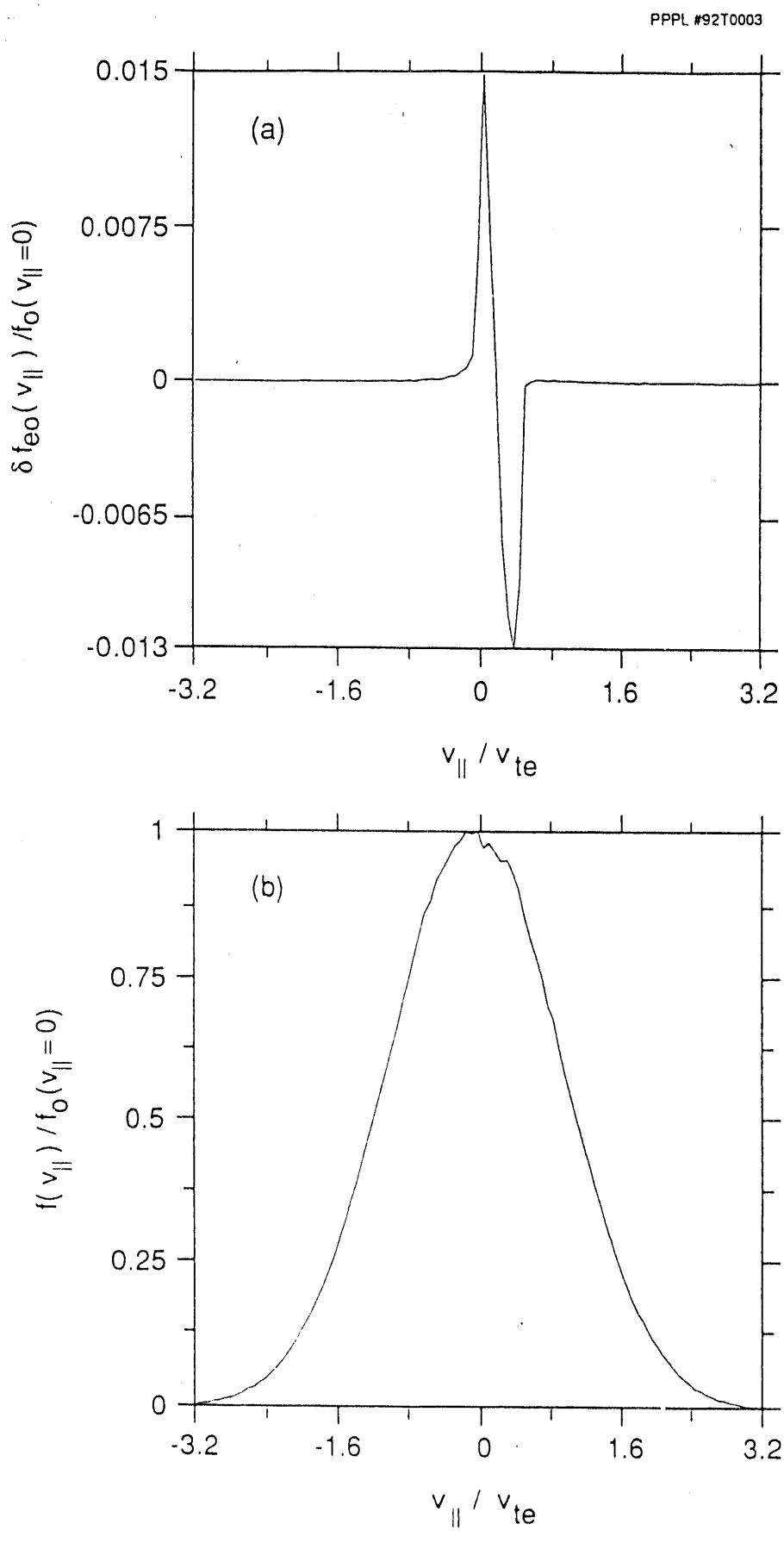
PPPL #92T0003
(a)
0.015
0.0075
0
-0.0065
-0.013
δ f_eo(v_||) /f_o(v_|| =0)
-3.2
-1.6
0
1.6
3.2
v_|| / v_te
(b)
1
0.75
0.5
0.25
0
f(v_||) / f_o(v_|| =0)
-3.2
-1.6
0
1.6
3.2
v_|| / v_te

Fig. 5

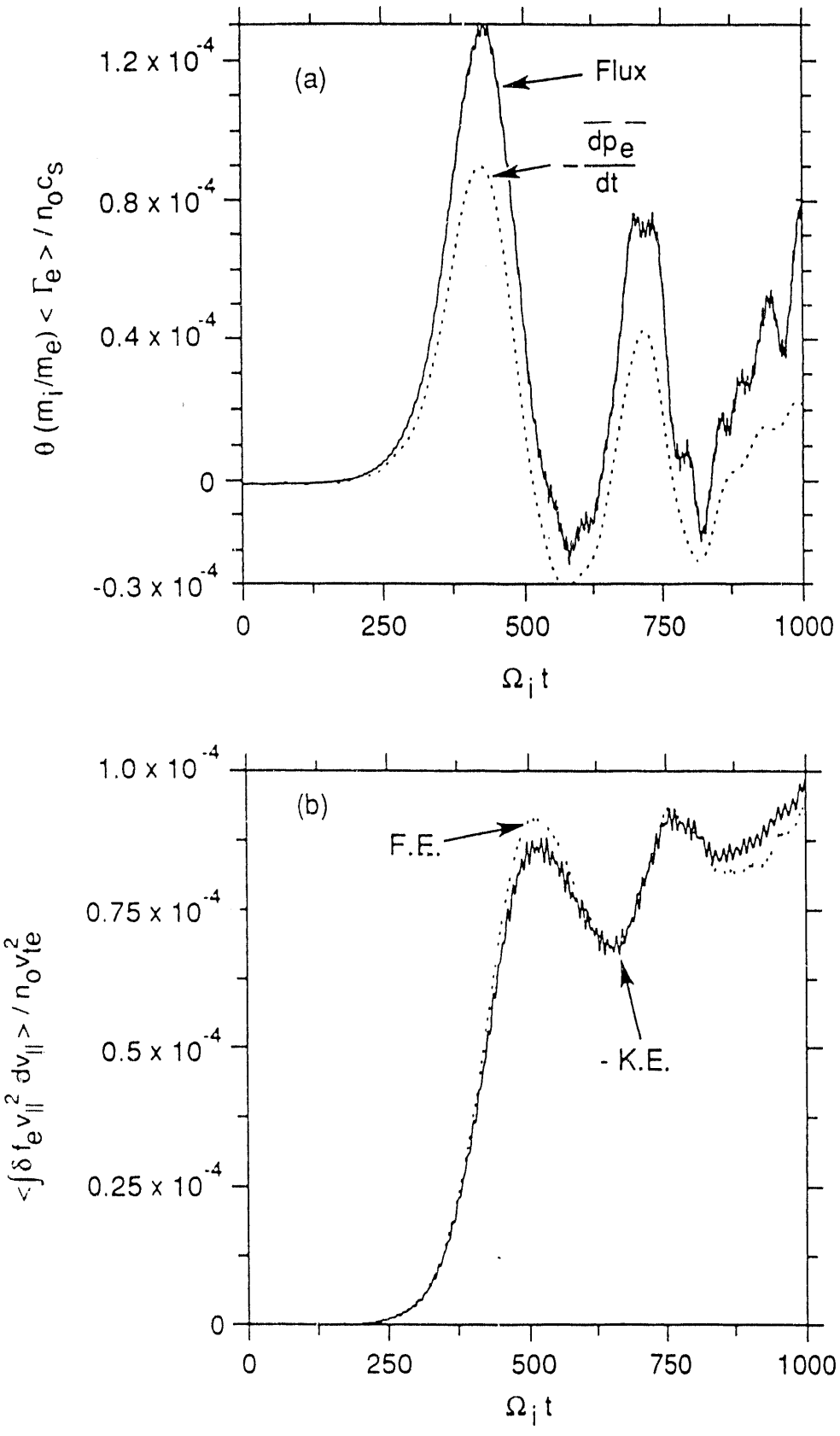
(a)
Flux
$-\overline{\frac{dp_e}{dt}}$
$\theta\,(m_i/m_e) < \Gamma_e > / n_o c_s$
1.2 x 10^{-4}
0.8 x 10^{-4}
0.4 x 10^{-4}
0
-0.3 x 10^{-4}
0
250
500
750
1000
$\Omega_i t$
(b)
F.E.
- K.E.
$< \int \delta f_e v_{||}^2 \, dv_{||} > / n_o v_{te}^2$
1.0 x 10^{-4}
0.75 x 10^{-4}
0.5 x 10^{-4}
0.25 x 10^{-4}
0
0
250
500
750
1000
$\Omega_i t$

Fig. 6

EXTERNAL DISTRIBUTION IN ADDITION TO UC-420

Dr. F. Paoloni, Univ. of Wollongong, AUSTRALIA
Prof. M.H. Brennan, Univ. of Sydney, AUSTRALIA
Plasma Research Lab., Australian Nat. Univ., AUSTRALIA
Prof. I.R. Jones, Flinders Univ, AUSTRALIA
Prof. F. Cap, Inst. for Theoretical Physics, AUSTRIA
Prof. M. Heindler, Institut für Theoretische Physik, AUSTRIA
Prof. M. Goossens, Astronomisch Instituut, BELGIUM
Ecole Royale Militaire, Lab. de Phy. Plasmas, BELGIUM
Commission-European, DG. XII-Fusion Prog., BELGIUM
Prof. R. Boucique, Rijksuniversiteit Gent, BELGIUM
Dr. P.H. Sakanaka, Instituto Fisica, BRAZIL
Instituto Nacional De Pesquisas Espaciais-INPE, BRAZIL
Documents Office, Atomic Energy of Canada Ltd., CANADA
Dr. M.P. Bachynski, MPB Technologies, Inc., CANADA
Dr. H.M. Skarsgard, Univ. of Saskatchewan, CANADA
Prof. J. Teichmann, Univ. of Montreal, CANADA
Prof. S.R. Sreenivasan, Univ. of Calgary, CANADA
Prof. T.W. Johnston, INRS-Energie, CANADA
Dr. R. Bolton, Centre canadien de fusion magnétique, CANADA
Dr. C.R. James,, Univ. of Alberta, CANADA
Dr. P. Lukác, Komenského Universzita, CZECHO-SLOVAKIA
The Librarian, Culham Laboratory, ENGLAND
Library, R61, Rutherford Appleton Laboratory, ENGLAND
Mrs. S.A. Hutchinson, JET Library, ENGLAND
Dr. S.C. Sharma, Univ. of South Pacific, FIJI ISLANDS
P. Mähönen, Univ. of Helsinki, FINLAND
Prof. M.N. Bussac, Ecole Polytechnique,, FRANCE
C. Mouttet, Lab. de Physique des Milieux Ionisés, FRANCE
J. Radet, CEN/CADARACHE - Bat 506, FRANCE
Prof. E. Economou, Univ. of Crete, GREECE
Ms. C. Rinni, Univ. of Ioannina, GREECE
Dr. T. Mual, Academy Bibliographic Ser., HONG KONG
Preprint Library, Hungarian Academy of Sci., HUNGARY
Dr. B. DasGupta, Saha Inst. of Nuclear Physics, INDIA
Dr. P. Kaw, Inst. for Plasma Research, INDIA
Dr. P. Rosenau, Israel Inst. of Technology, ISRAEL
Librarian, International Center for Theo Physics, ITALY
Miss C. De Palo, Associazione EURATOM-ENEA , ITALY
Dr. G. Grosso, Istituto di Fisica del Plasma, ITALY
Prof. G. Rostangni, Istituto Gas Ionizzati Del Cnr, ITALY
Dr. H. Yamato, Toshiba Res & Devel Center, JAPAN
Prof. I. Kawakami, Hiroshima Univ., JAPAN
Prof. K. Nishikawa, Hiroshima Univ., JAPAN
Director, Japan Atomic Energy Research Inst., JAPAN
Prof. S. Itoh, Kyushu Univ., JAPAN
Research Info. Ctr., National Instit. for Fusion Science, JAPAN
Prof. S. Tanaka, Kyoto Univ., JAPAN
Library, Kyoto Univ., JAPAN
Prof. N. Inoue, Univ. of Tokyo, JAPAN
Secretary, Plasma Section, Electrotechnical Lab., JAPAN
S. Mori, Technical Advisor, JAERI, JAPAN
Dr. O. Mitarai, Kumamoto Inst. of Technology, JAPAN
J. Hyeon-Sook, Korea Atomic Energy Research Inst., KOREA
D.I. Choi, The Korea Adv. Inst. of Sci. & Tech., KOREA
Prof. B.S. Liley, Univ. of Waikato, NEW ZEALAND
Inst of Physics, Chinese Acad Sci PEOPLE'S REP. OF CHINA
Library, Inst. of Plasma Physics, PEOPLE'S REP. OF CHINA
Tsinghua Univ. Library, PEOPLE'S REPUBLIC OF CHINA
Z. Li, S.W. Inst Physics, PEOPLE'S REPUBLIC OF CHINA
Prof. J.A.C. Cabral, Instituto Superior Tecnico, PORTUGAL
Dr. O. Petrus, AL I CUZA Univ., ROMANIA
Dr. J. de Villiers, Fusion Studies, AEC, S. AFRICA
Prof. M.A. Hellberg, Univ. of Natal, S. AFRICA
Prof. D.E. Kim, Pohang Inst. of Sci. & Tech., SO. KOREA
Prof. C.I.E.M.A.T, Fusion Division Library, SPAIN
Dr. L. Stenflo, Univ. of UMEA, SWEDEN
Library, Royal Inst. of Technology, SWEDEN
Prof. H. Wilhelmson, Chalmers Univ. of Tech., SWEDEN
Centre Phys. Des Plasmas, Ecole Polytech, SWITZERLAND
Bibliotheek, Inst. Voor Plasma-Fysica, THE NETHERLANDS
Asst. Prof. Dr. S. Cakir, Middle East Tech. Univ., TURKEY
Dr. V.A. Glukhikh,Sci. Res. Inst. Electrophys.I Apparatus, USSR
Dr. D.D. Ryutov, Siberian Branch of Academy of Sci., USSR
Dr. G.A. Eliseev, I.V. Kurchatov Inst., USSR
Librarian, The Ukr.SSR Academy of Sciences, USSR
Dr. L.M. Kovrizhnykh, Inst. of General Physics, USSR
Kernforschungsanlage GmbH, Zentralbibliothek, W. GERMANY
Bibliothek, Inst. Für Plasmaforschung, W. GERMANY
Prof. K. Schindler, Ruhr-Universität Bochum, W. GERMANY
Dr. F. Wagner, (ASDEX), Max-Planck-Institut, W. GERMANY
Librarian, Max-Planck-Institut, W. GERMANY
Prof. R.K. Janev, Inst. of Physics, YUGOSLAVIA

END

DATE FILMED

8/11/92